



# **Boron nitride inclusions within adhesive joints: Optimization of mechanical strength and bonded defects detection**

Matthias Barus, Hélène Weleman, Valérie Nassiet, Marina Fazzini,  
Jean-Christophe Batsale

## **► To cite this version:**

Matthias Barus, Hélène Weleman, Valérie Nassiet, Marina Fazzini, Jean-Christophe Batsale. Boron nitride inclusions within adhesive joints: Optimization of mechanical strength and bonded defects detection. International Journal of Adhesion and Adhesives, 2020, 98, pp.1-10. 10.1016/j.ijadhadh.2019.102531 . hal-03496058

**HAL Id: hal-03496058**

**<https://hal.science/hal-03496058>**

Submitted on 20 Dec 2021

**HAL** is a multi-disciplinary open access archive for the deposit and dissemination of scientific research documents, whether they are published or not. The documents may come from teaching and research institutions in France or abroad, or from public or private research centers.

L'archive ouverte pluridisciplinaire **HAL**, est destinée au dépôt et à la diffusion de documents scientifiques de niveau recherche, publiés ou non, émanant des établissements d'enseignement et de recherche français ou étrangers, des laboratoires publics ou privés.







OATAO is an open access repository that collects the work of Toulouse researchers and makes it freely available over the web where possible

This is an author's version published in: <http://oatao.univ-toulouse.fr/26994>

**Official URL:**

<https://doi.org/10.1016/j.ijadhadh.2019.102531>

**To cite this version:**

Barus, Matthias  and Weleman, Hélène  and Nassiet, Valérie   
and Fazzini, Marina  and Batsale, Jean-Christophe *Boron nitride inclusions within adhesive joints: Optimization of mechanical strength and bonded defects detection.* (2020) International Journal of Adhesion and Adhesives, 98. 1-10. ISSN 0143-7496

Any correspondence concerning this service should be sent  
to the repository administrator: [tech-oatao@listes-diff.inp-toulouse.fr](mailto:tech-oatao@listes-diff.inp-toulouse.fr)

Matthias Barus<sup>a</sup>, H  l  ne Weleman  <sup>a,\*</sup>, Val  rie Nassiet<sup>a</sup>, Marina Fazzini<sup>a</sup>, Jean-Christophe Batsale<sup>b</sup>

<sup>b</sup> I2M, Arts et Métiers ParisTech, Dpt. TREFLE, UMR-CNRS 5295, Bordeaux, France

**Keywords:**  
Epoxydes  
Composites  
Non-destructive testing  
Mechanical properties of adhesives

## 1. Introduction

In the case of CFRP bonded assemblies, the structural adhesive between inner and outer adherends is generally of same nature as the composite matrix (epoxy type). This configuration induces a weak thermal contrast between the different parts of the assembly and therefore limits the detection capacity of IRT techniques. In order to extend its scope of engineering applications, authors have recently proposed a specific device to improve the ability of active IRT to detect a bonded interface in such a context [8]. In this work, a step heating approach is used for exciting the specimen and the Differential Absolute Contrast (DAC) method [9] is employed for studying thermal contrasts induced on the surface of the structure. In addition to such experimental IRT procedure, authors have proposed to specifically design the joint material to better highlight bonded defects. They suggest to introduce high thermal conductivity particles to enhance flow transmission in virgin parts of assemblies. A comparison was done between alumina and Boron Nitride (BN) particles, two type of additives for which handling and dispersion inside the epoxy matrix can be done by conventional means. It was shown that BN particles provide the best performance for non-destructive inspection, leading to a higher contrast with a virgin assembly that significantly helps in capturing delaminations [10].

These previous studies have demonstrated the improvement of the

\* Corresponding author.  
E-mail address: [helene.weleman@enit.fr](mailto:helene.weleman@enit.fr) (H. Weleman).

IRT capability provided by conductive inclusions on the qualitative point of view. Yet, due to the material modification, mechanical properties of the new composite adhesive joint can be notably affected. Accordingly, quantitative investigation needs to be implemented to really validate the potential of the NDT-based design strategy for bonded interfaces analysis, specially to ensure its compliance with industrial requirements. Precisely, two questions arise: (i) To what extent do the additives inclusions affect the mechanical behaviour of the adhesive joint, (ii) To what extent do they improve the IRT detection capability? In the literature, these issues are often addressed separately. This work stands out by a dual analysis, which aims to find the best trade-off between mechanical and inspection requirements. In this way, the shear failure behaviour of the adhesive joint is first investigated via double strap lap shear tests for different BN volume fractions (Section 2). Since allowable delaminations may differ depending on engineering applications, IRT testing is carried out on defective assemblies for various controlled size debondings. With regard to the uncharged case, we were thus able to quantify the improvement in the detection capabilities of thermography according to the joint additives content (Section 3). Finally thermal data post-processing methods are implemented to optimize the defects detection limit size and get through mechanical requirements (Section 4).

## 2. Mechanical analysis

### 2.1. Materials and methods

Double strap lap shear test method is considered here to study the failure behaviour of the adhesive joint ([11,12]). Unlike single lap shear tests, such configuration reduces bending moments and allows to get close as possible to the shear behaviour of the adhesives. The inner and outer adherends are  $[0]_{11}$  (resp.  $[0]_5$ ) composite laminates, composed of Hexply® M79 with Torayca® T300 carbon fibers ( $0^\circ$  corresponds to Y axis). In view of composite plies thickness, thicknesses of inner and outer adherends have been adapted to better follow the ASTM standards (Fig. 1). Adherends are bonded with an epoxy glue (resin LY5052, hardener HY5052 from Huntsman®, average tensile modulus 2600 MPa and ultimate strength 60 MPa) loaded with BN particles (in form of platelets with an average size of  $8\mu\text{m}$ , Fig. 2-a). Thermo-physical properties of these materials are given in Table 1.

Several BN volume fraction  $f_a$  have been considered, namely:  $f_a = 0\%$  (BN0, epoxy matrix),  $f_a = 6\%$  (BN6),  $f_a = 12\%$  (BN12) and  $f_a = 18\%$  (BN18). A total of three specimens has been prepared for each configuration. In order to evenly disperse particles within the epoxy glue, a special care has been taken on the elaboration process. Indeed, due to the platelet form of particles, these ones have a natural tendency to flocculate during the mixing procedure. Two elaboration processes have been used depending on the BN particles percentage. Below  $f_a = 8\%$ :

(1) particles are blended with the matrix in two steps (50% of the total mass of BN each time); (2) the mixture is homogenized using a vibrating mixer; (3) the hardener is added and the mixture is homogenized again. Beyond  $f_a = 8\%$ : (1) 55% of the total mass of BN is blended step by step with the matrix; (2) the mixture is homogenized; (3) acetone (approximately 5% of the total mass of matrix) is introduced to decrease the mixture viscosity, before the addition of BN particles (approximately 10% of the total mass of matrix) and the homogenization phase; (4) step 3 is repeated until the remaining of BN particles is added. Once the mixing process is completed, air outflow is done under vacuum to ensure the most complete outflow of air bubbles in both elaboration processes. In order to control the particles dispersion, several SEM micrographs were done on surfaces of fractured BN/epoxy samples with additives content  $f_a = 18\%$  corresponding to the highest risk of agglomerates. As an example, Fig. 2-b illustrates the homogeneous distribution of BN additives inside the new joint.

Manufacturing double strap lap assemblies requires to ensure adhesive thickness calibration and homogeneity on the one hand and to avoid the flow of the adhesive on the adherends parts on the other hand. The first problem is solved using several composite wedges with adequate thickness, while the later is addressed by protecting adherends with Teflon sheets (Fig. 3). Each assembly is then held in position by five holding points and cured at  $80^\circ\text{C}$  during 15min inside an oven. Such cure cycle has been chosen to stand far from the glass transition temperature of the composite epoxy matrix ( $100 \pm 5^\circ\text{C}$ ). Masking Teflon sheet and wedges are removed from assemblies after curing.

Tensile tests are carried out with an Instron® 33R4204 machine (50 kN load sensor accurate at 0.25%, cross-head speed of  $1.27\text{ mm}\cdot\text{min}$ ). During tests, specimens are mainly subjected to plane strains in the YZ plane since the thickness (along Z) of the specimen is much smaller than its width (along X, Fig. 1). Therefore, 2D Digital Image Correlation (DIC) technique is used for measuring the surface displacement fields at the free edge of the adhesive. Strain analysis is conducted using the Gom optical measurement system Aramis 2 M with a resolution of  $1624 \times 1236$  pixels; frequency acquisition is settled to 4 Hz in regards to the large amount of acquired data. Measurement distance is approximately 140 mm so as to follow the adhesive during all the test and the studied area is  $16.4 \times 12.5\text{ mm}$  which leads to a spatial resolution (pixel size) of around  $0.01\text{ mm}$  (Figs. 1, 4-b). Samples are painted using white and black matt paint to create a speckle pattern which is tracked by DIC. Due to the image resolution, the thickness of the adhesive is covered by around 40 pixels and a total of 4 neighbouring pixels groups are used to define the shear strains within the joint.

### 2.2. Experimental results and discussion

Regarding displacements acquisition during the tests, DIC measurements show a quite uniform stress distribution up to failure (Fig. 5).

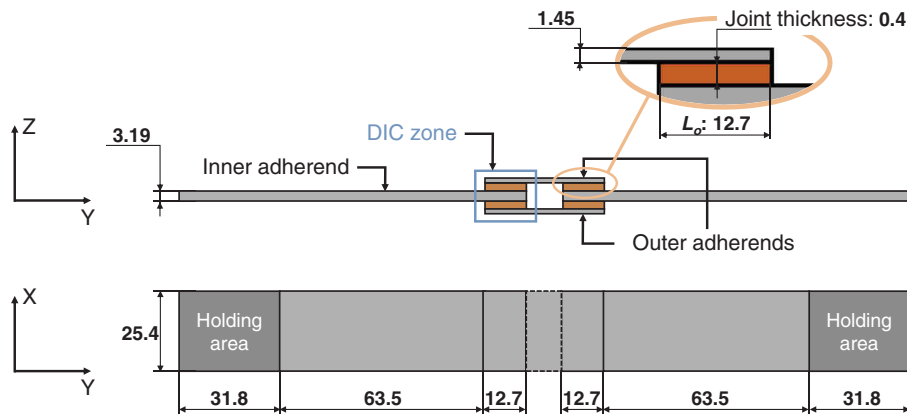


Fig. 1. Geometry of a double strap lap shear test assembly (lengths in mm).

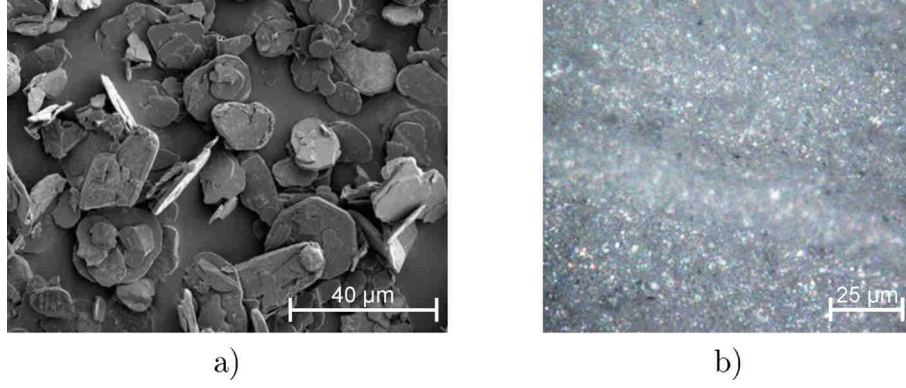


Fig. 2. SEM micrographs: (a) BN particles, (b) spatial distribution of BN particles (white) inside epoxy matrix (grey) for BN18 case.

Table 1

Thermo-physical properties of used materials.

	$\rho$ [kg·m <sup>-3</sup> ]	$C_p$ [J·kg <sup>-1</sup> ·K <sup>-1</sup> ]	$\lambda$ [W·m <sup>-1</sup> ·K <sup>-1</sup> ]
Composite ply (0°) [8]	1550	883	$\lambda_a = 3.05\lambda_l = 0.51$
Epoxy glue [8]	1172	1317	0.226
BN particles [13]	2280	1610	300

Shear strains  $\varepsilon_{YZ}$  of right and left interfaces are equal in absolute value since the structure is symmetric in regards with the XY plane. Yet, they are of opposite sign due to the relative Y direction displacement of the inner and outer adherends and related shear stresses  $\tau_{YZ}$  (Fig. 6). Then, all the four bonded interfaces of each specimen have failed for all tested assemblies and whatever the BN content. Precisely, failure facies are typical of adhesive testing (Fig. 7): adhesive failure for which the failure

occurs at the interface between the joint and the adherend, cohesive failure for which the cracking concerns the adhesive and a mixed mode. Yet, it is important to note that most of the tests lead to cohesive failure, namely 69% of the fracture surface for BN0, 75% for BN6, 92% for BN12 and 100% for BN18, is of cohesive type. It seems thus that the experimental design is relevant to provide the adhesive mechanical behaviour.

Fig. 8 provides the mechanical response of adhesive epoxy for different BN volume fractions  $f_a$ . Regarding stress-displacement curves (Fig. 8-a), similar tendency can be seen for different specimens. Yet, failure behavior clearly differs according to particle loading. With increasing BN content, shear displacement at failure is clearly reduced. The wider range of DIC shear strains at small  $f_a$  ( $\pm 2.25\%$  for BN0 and  $\pm 0.07\%$  for BN18, Fig. 5) corroborates the loss of ductility induced by BN additives. At the same time, an increase of the BN particles content leads to a significant reduction of failure strength (Fig. 8-b). For instance with a BN volume fraction  $f_a = 18\%$  (BN18), one gets a decrease of 53% of the failure strength compared to epoxy case (BN0). The higher rigidity of BN

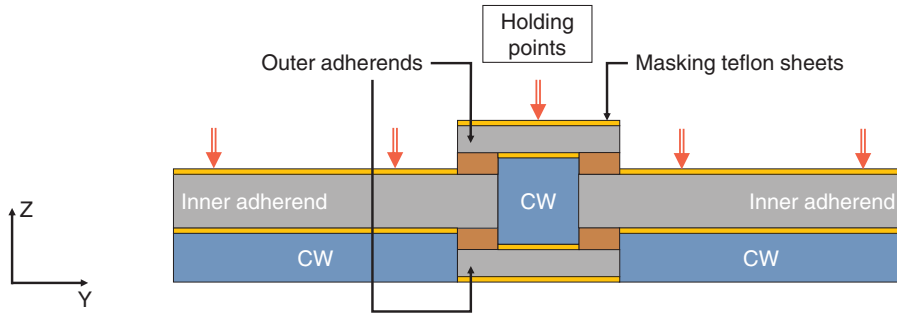


Fig. 3. Schematic representation of the assembly during curing (CW: composite wedges).

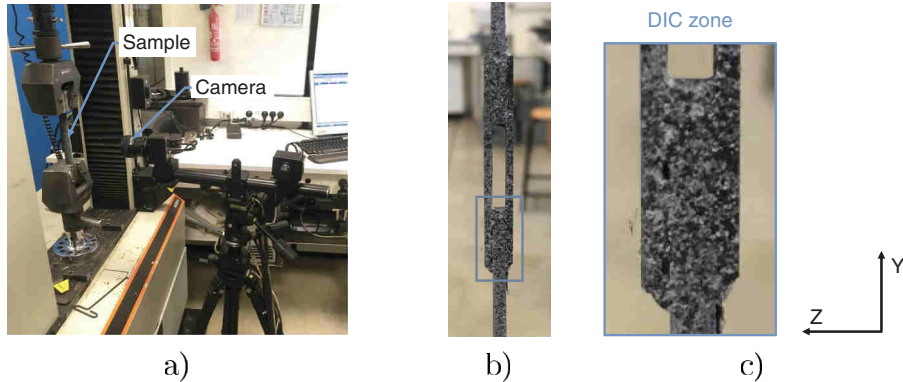


Fig. 4. Experimental set-up for the double strap lap shear tests study: (a) testing and DIC set-up, (b) entire sample and (c) DIC studied area.

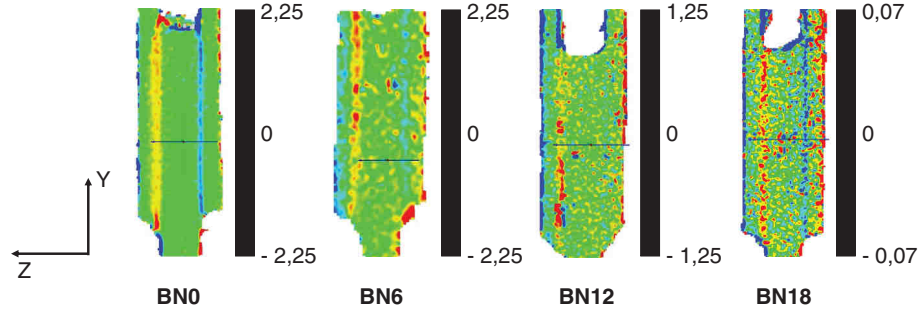


Fig. 5. Experimental shear strain (%) at failure of double strap lap shear assemblies according to BN content.

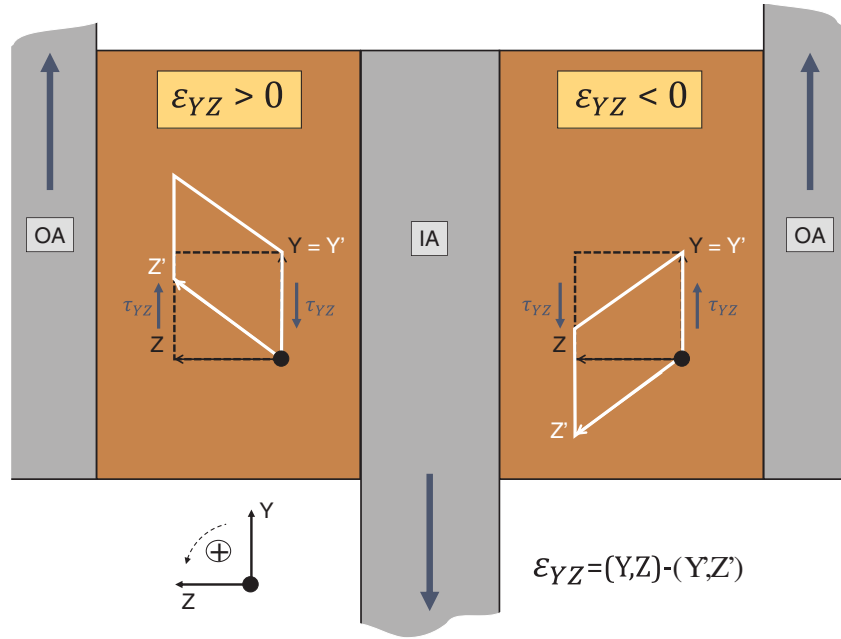


Fig. 6. Schematic representation of shear load inside each interface of the assembly and related shear strain  $\varepsilon_{YZ}$  signs (IA: inner adherend, OA: outer adherend).

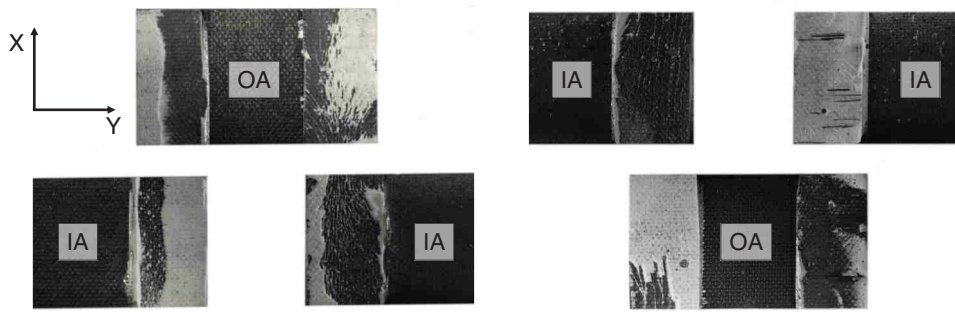
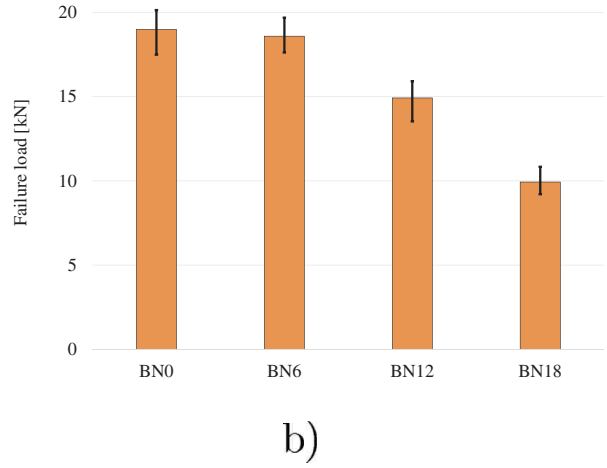
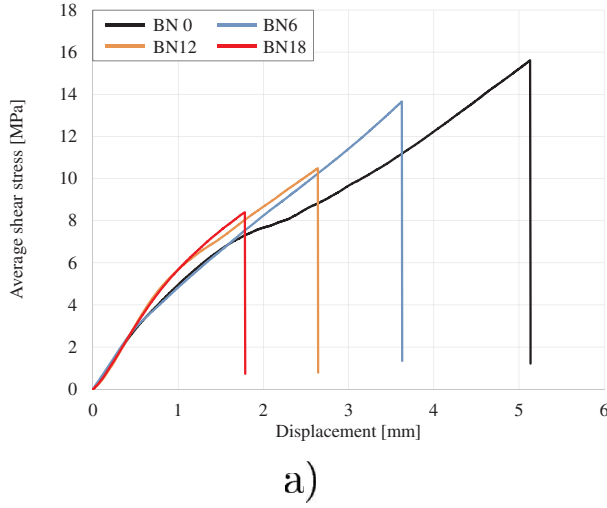


Fig. 7. Typical failure facies of assembly with inner adherend (IA) and outer adherend (OA) (BN6 case, BN loaded epoxy is white).

particles compared to epoxy probably plays a major role in such increase of the brittleness of the joint while increasing  $f_a$ . Indeed, it was shown by Zhou et al. [14] that increasing particles content can lead to the creation of voids or interfacial defects and consequently to the decrease of the tensile strength. Moreover, a high filler content can generate agglomerations, obstruct the polymer chain mobility and thus induce a weaker elongation at break [15].

From these results, it seems thus important not to exceed a certain proportion of BN particles inside the adhesive in order to ensure its

mechanical reliability. At the same time, increasing values of  $f_a$  tend to exacerbate thermal contrasts and to improve the bonding defects detection [10]. Now the issue is thus to qualify the ability of IRT to detect defects in bonded assemblies according to the BN volume fraction of adhesive joint. Precisely, we intend to determine the size of the critical defect that can be detected by IRT as a function of the BN content. So as to keep reasonable mechanical performances compared to BN0, namely less than 25% reduction of the yield strength, only proportions of less than  $f_a = 12\%$  are considered in what follows, namely



**Fig. 8.** Mechanical behaviour of composite bonded assemblies for different BN volume fractions: (a) typical average shear stress-displacement curves (b) failure loads (mean values and standard deviation).

BN0, BN6 and BN12 configurations.

### 3. IRT non destructive analysis

#### 3.1. Materials and methods

The influence of the adhesive joint thermal properties onto the ability of IRT to detect bonded defects is studied on two  $[0]_5$  CFRP laminates linked together by an adhesive joint including controlled size bonded defects (Fig. 9-a). An original approach has been set up to introduce artificial defects. Before spreading adhesive joint material,

stacks of Teflon sheets (with calibrated thickness) are used to mask cylindrical (diameter  $\varphi$ , height corresponding to the adhesive thickness) areas on the bottom adherend. The question of allowable size of defects for materials and structures remains quite open and depends on the several parameters (materials, geometry, engineering applications). Accordingly, different diameters  $\varphi$  have been considered, namely  $\varphi = 15$  mm (defect n°1),  $\varphi = 13$  mm (defect n°2),  $\varphi = 9$  mm (defect n°3) and  $\varphi = 6$  mm (defect n°4), in order to evaluate the IRT capacity (Fig. 9-a, 9-b). The adhesive joint thickness is also controlled by Teflon sheets (Fig. 9-b) and uniformity of the joint thickness is ensured by means of a tape casting machine. The device used for spreading glue on surfaces is a

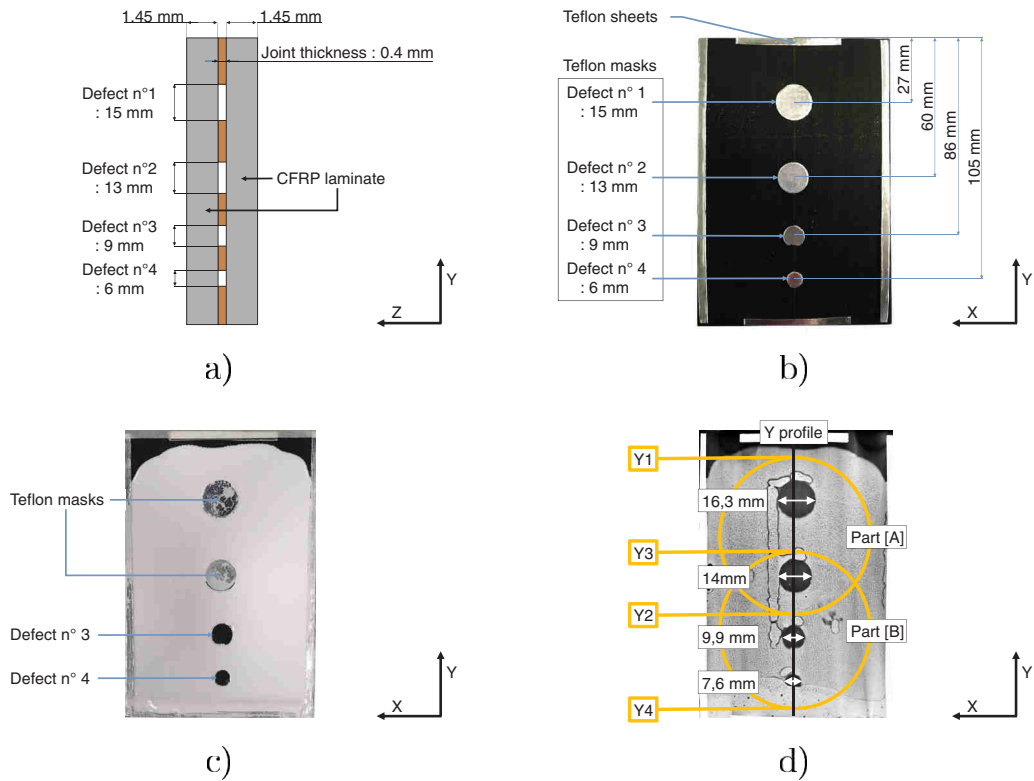


**Fig. 9.** CND sample fabrication: (a) schematic representation of the defective bonded assembly, (b) defects creation, (c) removing of masks here for defects n°3 and n°4, (d) tomographic slice of the sample geometry after curing.



current doctor blade which has been equipped with an automatic speed control system. This latter development was carried out in the laboratory and allows to define precisely the constant spread rate to minimize the porosity within the joint. Teflon masks are then removed to create bonded defects (Fig. 9-c) and the upper coupon is placed on the assembly. After curing, geometry of defective assemblies is checked using X-ray tomography (Easytom RX Solutions tomograph with X-Act software, tension of 115 kV, intensity of 260  $\mu$ A). Tomographic slices are acquired with a flat panel detector  $1920 \times 1536$  pixels leading to a voxel size of 76  $\mu$ m. As illustrated on Fig. 9-d, defects localization and size are very closed to expected ones.

The active IRT procedure recently developed by authors uses a specific experimental device specially designed to control tests conditions (Fig. 10). Thermal load of samples is conducted using a halogen lamp (maximum power of 1000W) associated with an optical set-up to deliver a homogeneous heating on a (quasi circular) thermally stressed area (heat flow intensity of  $500\text{W}\cdot\text{m}^{-2}$  [8]). Precisely, a step heating approach is considered with a thermal stimulation of 10s. Furthermore, environmental effects are minimized by painting the studied surfaces in mat black and by using DAC:  $\Delta T(t) = T(t) - T_0(t=0)$ , with  $T$  and  $T_0$  respectively the current (at time  $t$ ) and initial temperature field [9]. Thermal acquisition is performed using a FLIR® Titanium retrofitted camera (InSb sensors that operate in the 3.5 to 5  $\mu$ m waveband, thermal sensitivity of 25 mK at 30°C, lens with 50 mm of focal length and a pixel resolution of  $320 \times 256$  pixels, frame rate of 50 Hz) associated with Altair software. The detailed design of the test procedure and choices justification can be found in Ref. [8]. Note that the glass transition temperature of the adhesive is equal to  $75 \pm 2^\circ\text{C}$  for considered cure conditions. Since the surface temperature elevation is less than  $10^\circ\text{C}$  during the heating phase, the IRT procedure does not modify the adhesive microstructure.

### 3.2. Experimental results

Due to the size of the heated area (average diameter of 68.5 mm), the full analysis of samples is done in two parts: part [A] covers defects n°1 and n°2, while part [B] concerns defects n°2, n°3 and n°4 (Fig. 9-d). Fig. 11 shows the local temperature variation related to Y measurement profile for part [A] according to BN content at the end of the heating phase ( $t = 10\text{s}$ ).

Through this first analysis, it is possible to distinguish inside the heated area (between points Y1 and Y2, Fig. 9-d) the local temperature increase induced by the two biggest defects (n°1,  $\varphi = 15\text{ mm}$  and n°2,  $\varphi = 13\text{ mm}$ ) for all specimens. To improve the results interpretation, a post-processing method that isolates the specific defect response has been used [8]. Precisely, the relative temperature variation  $\Delta T_2(t) = \Delta T_{\text{assembly}}(t) - \Delta T_{\text{mono}}(t)$  is obtained by subtracting from the thermal field variation  $T_{\text{assembly}}(t)$  of the bonded assembly the thermal field

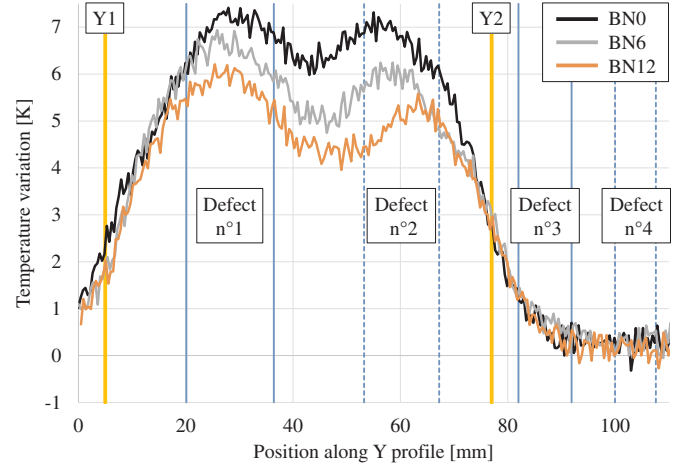


Fig. 11. Experimental temperature variation  $\Delta T$  along Y profile at the end of the heating phase for BN0, BN6 and BN12 samples (part [A]).

variation  $T_{\text{mono}}(t)$  obtained at the same time  $t$  for an equivalent but monolithic (non bonded) sample (same material geometry and same global thickness, Fig. 12). By this way, it is very easy to capture the two biggest defects for all samples whatever the BN content (Fig. 13-a). For the detection of bonding defects bigger than 13 mm at 1.45 mm depth inside the assembly, the modification of adhesive thermal properties is thus not necessary. In other terms, this class of defects can be captured in assemblies bonded with the basic epoxy matrix (BN0).

In contrast, the part [B] investigation, covering smaller defects (specially n°3,  $\varphi = 9\text{ mm}$  and n°4,  $\varphi = 6\text{ mm}$ ), is clearly more difficult (Fig. 13-b). In several cases, the local temperature peaks induced by small defects are too diffuse and cannot be distinguished directly from the relative field  $\Delta T_2$ . If the  $f_a = 12\%$  proportion makes it possible to identify almost all defects, only defects bigger than 9 mm appear in the case of BN6 and defects smaller than 13 mm cannot be seen with BN0. As expected, it is demonstrated that the limit size for defect detection by IRT depends on the additives content.

According to the mechanical investigation (section 2) and these results, the optimal BN content represents a trade-off between adhesion efficiency and NDT issues. For instance, the detection of the 6 mm defect with the current procedure would require the use of BN content  $f_a = 12\%$  and would thus lead to a strong degradation of the bonded mechanical strength ( $-25\%$  compared to BN0). The solution considered in what follows is to focus efforts on the post-processing method of thermal fields. The objective is to improve the detection limit for a given  $f_a$ , or, equivalently, reduce the BN content necessary to detect given size defects.

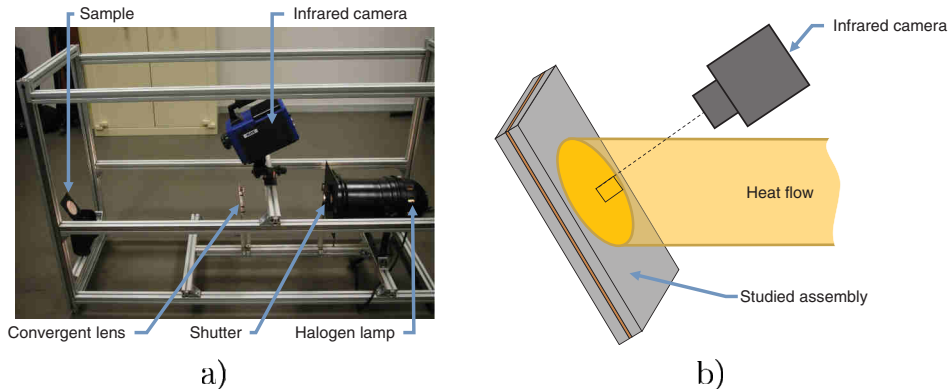


Fig. 10. Specific thermal device: (a) thermal bench, (b) schematic representation of the thermal load [8].



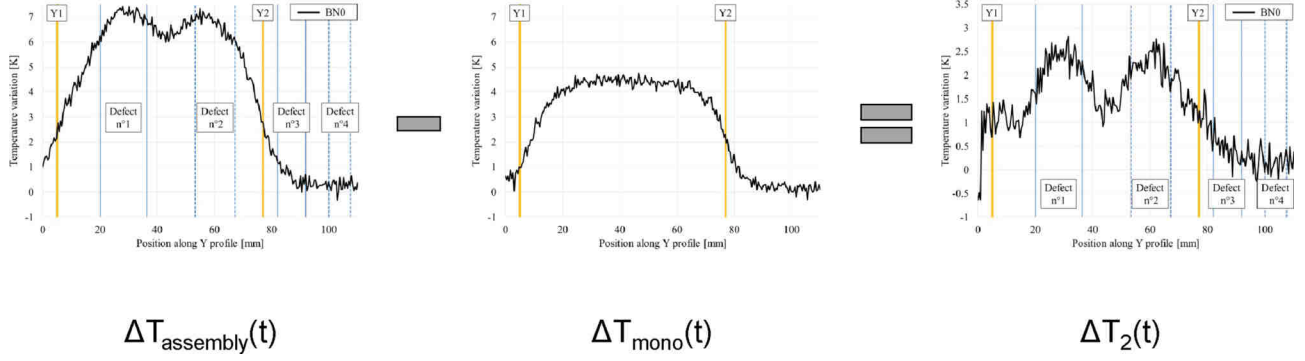


Fig. 12. Example of  $\Delta T_2(t)$  post-processing (part [A], BN0 case).

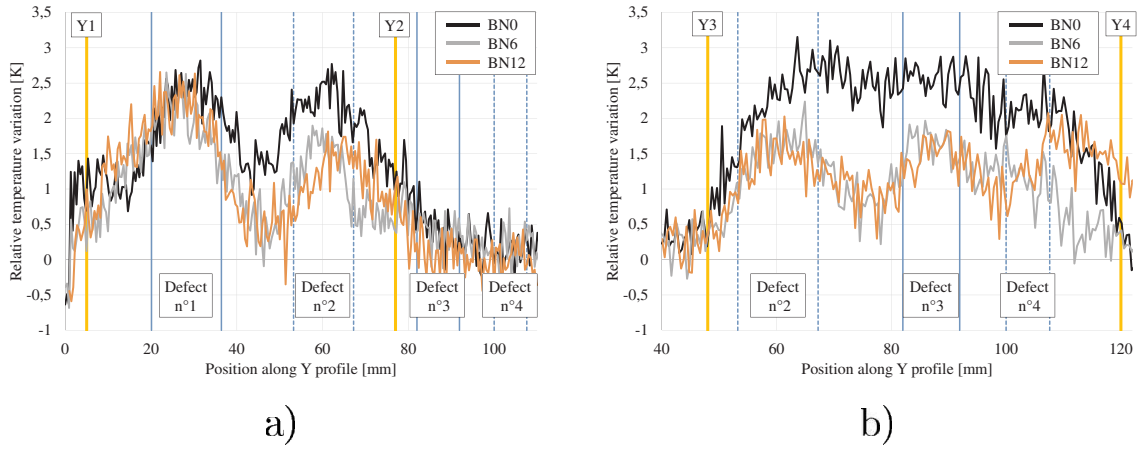


Fig. 13. Experimental relative temperature variation  $\Delta T_2$  along Y profile at the end of the heating phase for BN0, BN6 and BN12 samples: (a) part [A], (b) part [B].

#### 4. Thermal data post-processing

To enhance the specific thermal response of bonded defects, Singular Values Decomposition (SVD) appears as an interesting solution. Such method has been commonly used for many years in numerical linear algebra, with several applications in thermal analysis [9,16], image processing [17] and for reducing the size of data [18]. In thermal analysis, SVD is an alternative tool allowing to extract significant data from a matrix in a compact and simplified manner. More generally, it can be considered as an eigen-method applicable to non-squared matrices. The SVD of a matrix  $A \in \mathbb{R}^{m \times n}$  such that  $m \geq n$  is given by  $A = U\Sigma V^T$  where  $U \in \mathbb{R}^{m \times m}$  and  $V \in \mathbb{R}^{n \times n}$  are orthogonal matrixes ( $T$  stands for the transpose). The matrix  $\Sigma \in \mathbb{R}^{m \times n}$  has non negative diagonal elements appearing in decreasing order ( $0$  is the zero matrix with appropriate dimensions):

$$\Sigma = \begin{bmatrix} \Xi \\ 0 \end{bmatrix}, \quad \Xi = \text{diag}\{\sigma_1 \geq \sigma_2 \geq \dots \geq \sigma_n \geq 0\} \quad (1)$$

Diagonal entries of  $\Xi$  are called the singular values of  $A$ , while the matrices  $U$  and  $V$  correspond to the left and right singular vectors of  $A$ . Practically,  $\sigma_i$  correspond to eigen values of product  $AA^T$  (or equivalently  $A^T A$ ),  $U$  (respectively  $V$ ) corresponds to the matrix of eigenvectors of  $AA^T$  (resp.  $A^T A$  [19]).

In this study, such decomposition is applied to the relative thermal field, namely  $A = \Delta T_2$ , using Matlab® software. Precisely, the experimental procedure leads to an acquisition area of  $(m = 256) \times (n = 192)$  pixels. As thermal data fully exhibit noise perturbation, it may be more interesting to apply the Truncated SVD technique (TSVD) obtained by truncating the SVD development at a given degree  $r < n$ , namely  $A_r = U\Sigma_r V^T$  with:

$$\Sigma_r = \begin{bmatrix} \Xi_r \\ 0 \end{bmatrix} \quad (2)$$

$\Xi_r$  corresponds to the diagonal matrix built upon  $\Xi$  such that  $\sigma_j = 0$  for  $j = r + 1, n$ . The optimal degree  $r$  able to reduce noise while keeping the significant part of the initial signal is defined here by applying TSVD for increasing degrees  $r$  until the stabilization of the norm  $L_r = \max_{i=1, m} \sum_{j=r+1}^n$

$| (A_r)_{ij} |$  of matrix  $A_r$  (Fig. 14-a). Considering the criterion  $\left| \frac{L_r - L_{r+1}}{L_r} \right| \leq 10^{-3}$ ,

Fig. 14-b illustrates the denoising operation applied on the relative thermal field  $\Delta T_2$  at the end of the heating phase ( $t = 10s$ ) for the BN6 case. Such post-processing allows an improvement for NDT detection as it makes it possible to properly identify bonded defects n°2 ( $\varphi = 13$  mm) and n°3 ( $\varphi = 9$  mm) for a BN proportion acceptable on the mechanical point of view.

In spite of the noise reduction, access to the 6mm defect still remains a difficult task, that may be attributed to the focus of the SVD decomposition on a given time. Therefore, it is proposed to additionally set up the Principal Component Thermography (PCT) technique that helps to enhance significant features of a signal by providing the strongest projection for both spatial and temporal evolutions [20]. Denoting  $n_k$  the number of 2D matrices  $A(t) \in \mathbb{R}^{m \times n}$  during a time period, such method first requires to build a unique matrix  $A' \in \mathbb{R}^{(m \times n) \times n_k}$  by rearranging time variations along columns in  $A'$  and spatial variations along its rows (Fig. 15). From this, application of SVD on matrix  $A'$  provides interesting results for data interpretation: columns of left singular vector  $U' \in \mathbb{R}^{(m \times n) \times (m \times n)}$  of  $A'$ , called Empirical Orthogonal Functions (EOF), correspond to orthogonal statistical modes that describe spatial

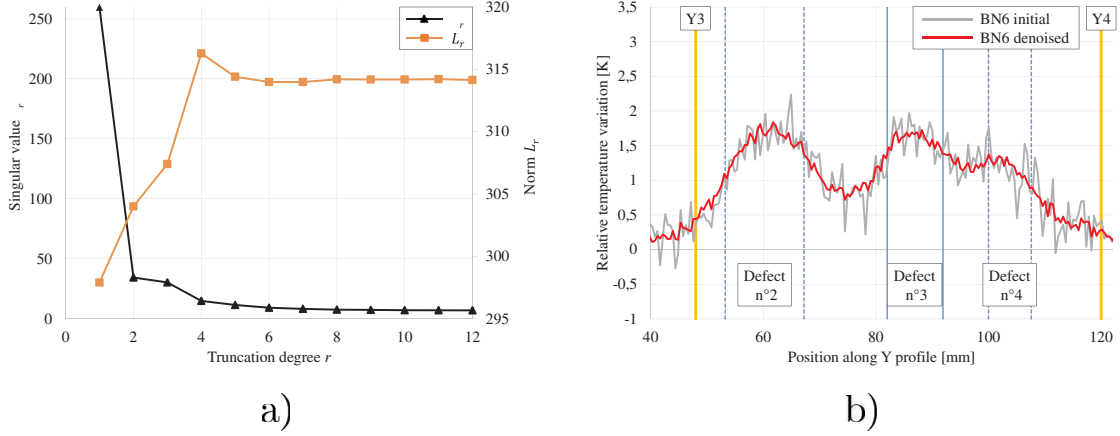


**Fig. 14.** TSVD operation applied on relative temperature variation  $\Delta T_2$  at the end of the heating phase for BN6 (part [B]): (a) singular values  $\sigma_r$  and matrix norm  $L_r$  according to truncation degree  $r$ , (b) experimental and denoised ( $r = 8$ )  $\Delta T_2$  evolution along Y profile.

variations of data, while rows of right singular vector  $V^r \in \mathbb{R}^{n_k \times n_k}$  of  $B^r$ , called Principal Component (PCs), account for time variations.

In the present case, PCT operation is applied to TSVD-processed 2D matrixes  $A = \Delta T_{2r}(t)$  with adequate  $r$  (satisfying the norm criterion) for each  $t$ . Thermal fields have been acquired from  $t = 0$ s to  $t = 20$ s with 50 Hz infrared camera, accordingly,  $n_k = 1000$ . Regarding time variations, PC vectors help to identify times that correspond to most significant global signal evolutions. Here, the end of the heating phase ( $t = 10$ s) appears as a key point (see Fig. 16-a), such choice was thus relevant for previous SVD analyses. Yet, the consideration of EOF modes provides a more meaningful interpretation through the integration of all significant signal evolutions over both space and time. In agreement with other thermal studies [9,20], variability of the data is concentrated in leading principal modes. Indeed, first three modes accounts for 98.3% of the variation in the raw data, while the primary mode alone accounts for 96.3%. Precisely, secondary mode EOF<sub>2</sub> accounts for the homogeneous part of the signal (see Y profile derived from such thermal on Fig. 16-c) whereas primary EOF<sub>1</sub> and third EOF<sub>3</sub> modes show its contrasting part (Fig. 16-b and 16-d). If the later modes are thus consistent with thermal heterogeneities induced by internal defects, their respective response is proportional to the extent of debonded areas: EOF<sub>1</sub> accounts for most significant contrasts and highlights biggest defects, while EOF<sub>3</sub> makes it

possible to capture less significant varying features related to smallest defects, specially n°3 with  $\varphi = 9$  mm and n°4 with  $\varphi = 6$  mm. Denoising operation applied to EOFs vectors even provides a clearer visualization of these results (see Fig. 16-b to d).

## 5. Conclusions

Introducing boron nitride conductive particles within epoxy joint helps the IRT investigation of internal defects within bonded assemblies. This study has first intended to characterize the resulting mechanical behaviour of the loaded joint using double strap lap shear tests. It is demonstrated that increasing BN content leads to a significant reduction of failure strength of the adhesive joint and consequently of the reliability of bonded assemblies. So as to find the best compromise between NDT and mechanical requirements, an active thermal procedure was applied on composite assemblies affected by controlled size bonding defects. The interest of the signal data processing to enhance thermal contrasts and decrease the limit in size detection is clearly illustrated. Specially, eigen-values decompositions such as SVD and PCT appear as relevant solutions. For instance, it is shown that a 6% BN content inside the epoxy joint makes it possible to capture  $\varphi = 6$  mm size defects at 1.45 mm depth inside carbon-epoxy bonded composites while ensuring

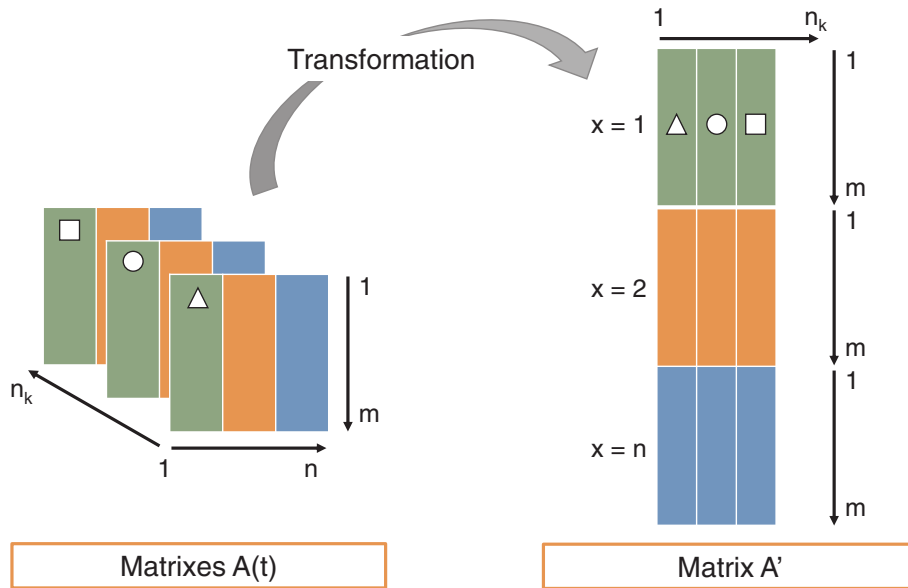


**Fig. 15.** Reorganization of the temporal matrixes into a 2D matrix.

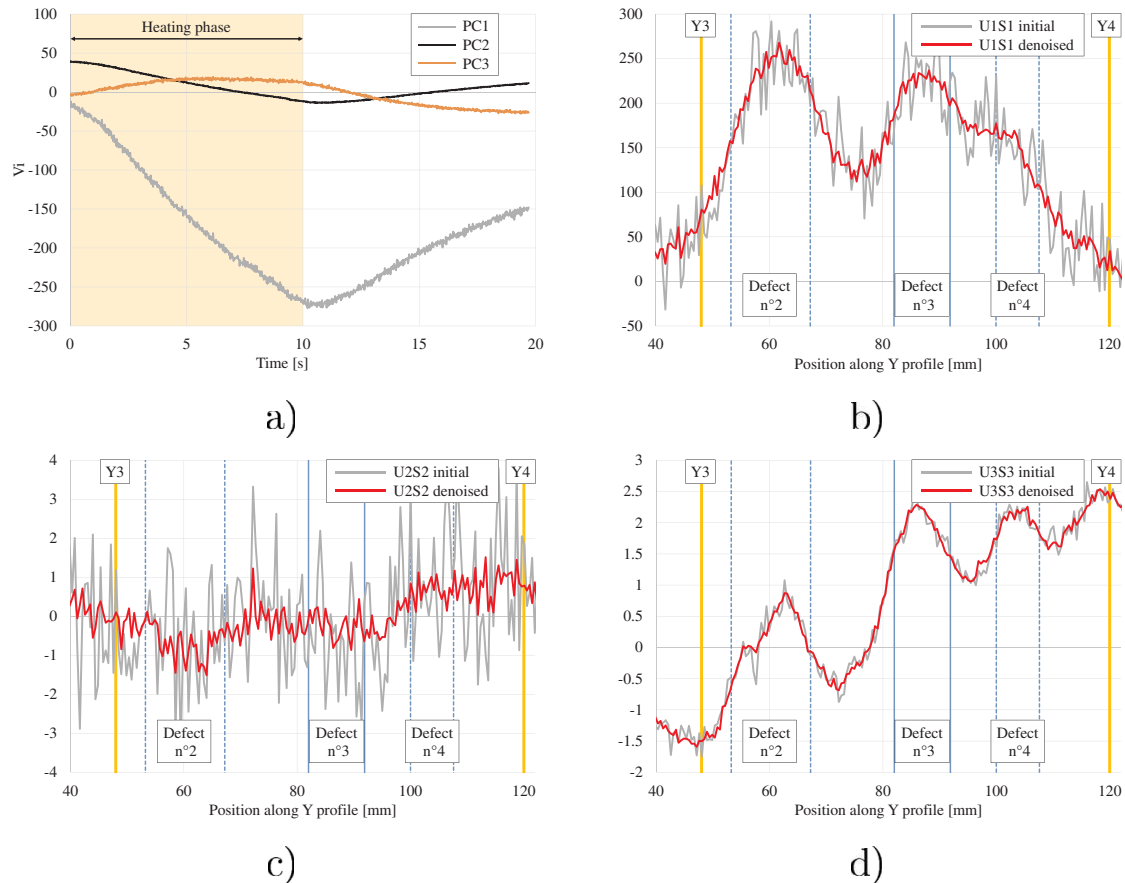


**Fig. 16.** PCT operation applied on TSVD-processed relative temperature variation  $\Delta T_2$  for BN6 (part [B]): (a) Leading first PC vectors, (b) EOF<sub>1</sub> ( $\sigma_1 = 6079$ ), (c) EOF<sub>2</sub> ( $\sigma_2 = 587$ ), (d) EOF<sub>3</sub> ( $\sigma_3 = 481$ ).

good mechanical performances of assemblies.

To go further, it will be really interesting to work on the type and size of conductive particles but also on the use of a coupling agent (like silane) which can either improve NDT detection or limit mechanical consequences, or even both. Specially, carbon-based particles (graphite, nano-tubes, graphene) would be of great interest with very high conductivity (thus stronger contrasts) and better compatibility with epoxy matrix if mixture homogeneity can be ensured. Therefore, the methodology described in this paper will extend even more the scope of IRT capabilities. Another relevant point concerns the criterion used to build a trade-off between mechanical and NDT performances. The investigation of mechanical performances of defective bonded assemblies with BN-loaded adhesive would help to clearly define the critical size of defect that cause significant strength degradation for a given configuration of assembly (materials and geometry) and engineering application. Such an analysis would help to refine the compromise solution considered in this approach.

## Acknowledgements

The authors wish to thank the reviewers for their comments and suggestions that significantly helped to improve the paper.

## References

- [1] Adams RD, Drinkwater BW. Nondestructive testing of adhesively-bonded joints. *NDT E Int* 1997;30:93–8.
- [2] Baker A, Gunnion JA, Wang J. On the certification of bonded repairs to primary composite aircraft components. *J Adhes* 2015;91:4–38.
- [3] Amenabar I, Mendikute A, López-Arraiza A, Lizaranzu M, Aurrekoetxea J. Comparison and analysis of non-destructive testing techniques suitable for delamination inspection in wind turbine blades. *Comp Part B* 2011;42:1298–305.
- [4] Balageas D, Maldague X, Burleigh D, Vavilov VP, Oswald-Tranta B, Roche JM, Pradere C, Carlomagno GM. Thermal (IR) and other NDT techniques for improved. *Mater Insp J Nondestruct Eval* 2016;35:18.
- [5] Asif M, Khan MA, Khan SZ, Choudhry DS, Khan KA. Identification of an effective nondestructive technique for bond defect determination in laminate composites - a technical review. *J Compos Mater* 2018;52:3589–99.
- [6] Genest M, Martinez M, Mrad N, Renaud G, Fahr A. Pulsed thermography for non-destructive evaluation and damage growth monitoring of bonded repairs. *Compos Struct* 2009;88:112–20.
- [7] Palumbo D, Tamborrino R, Galiotti U, Aversa P, Tati A, Luprano VAM. Ultrasonic analysis and lock-in thermography for debonding evaluation of composite adhesive joints. *NDT E Int* 2016;78:1–9.
- [8] Barus M, Welemane H, Collombet F, Pastor ML, Cantarel A, Crouzeix L, Grunevald YH, Nassiet V. Bonded repair issues for composites: an investigation approach based on infrared thermography. *NDT E Int* 2017;85:27–33.
- [9] Ibarra-Castaneda C, Piau JM, Guilbert S, Avdelidis NP, Genest M, Bendada A, Madalag XVP. Comparative study of active thermography techniques for the non destructive evaluation of honeycomb structures. *Res Nondestruct Eval* 2009;1: 31–20.
- [10] Barus M, Welemane H, Nassiet V, Pastor ML, Cantarel A, Collombet F, Crouzeix L, Grunevald YH. NDT-based design of joint material for the detection of bonding defects by infrared thermography. *NDT E Int* 2018;93:157–63.
- [11] Marques EAS, da Silva LFM. Joint strength optimization of adhesively bonded patches. *J Adhes* 2008;84:915–34.
- [12] ASTM 3528. Standard test method for strength properties of double lap shear adhesive joints by tension loading. 2016.
- [13] Zhu B, Ma J, Wu J, Yung KC, Xie CS. Study on the properties of the epoxy-matrix composites filled with thermally conductive AlN and BN ceramic particles. *J Appl Polym Sci* 2010;118:2754–64.
- [14] Zhou W, Zuo J, Zhang X, Zhou A. Thermal, electrical, and mechanical properties of hexagonal boron nitride-reinforced epoxy composites. *J Compos Mater* 2014;48: 2517–26.
- [15] Öner M, Kizil G, Keskin G, Pochat-Bohatier C, Bechelany M. The effect of boron nitride on the thermal and mechanical properties of Poly(3-hydroxybutyrate-co-3-hydroxyvalerate). *Nanomater Basel* 2014;8:940.

- [16] Guo Q, Zhang C, Zhang Y, Liu H. An efficient SVD-based method for image denoising. *IEEE T Circ Syst Vid* 2016;26:868–80.
- [17] Protter M, Elad M. Image sequence denoising via sparse and redundant representations. *Soc Indus Appl Math IEEE T Image Process* 2009;27:35–46.
- [18] Yahia AA, Palomo Del Borrio E. Thermal systems modelling via singular value decomposition: direct and modular approach. *Appl Math Model* 1999;23:447–68.
- [19] Golub GH, Van Laon CF. *Matrix computations*. third ed. Baltimore and London: The Johns Hopkins University Press; 1996.
- [20] Rajic N. Principal component thermography for flaw contrast enhancement and flaw depth characterisation in composite structures. *Compos Struct* 2002;58: 521–8.